MSW MANAGEMENT -Multidisciplinary, Scientific Work and Management Journal
ISSN: 1053-7899
Vol. 36 Issue 1, 2026, Pages: 1862-1871

Classifying Attention Deficit Hyperactivity Disorder (ADHD) through MRI images by Fuzzy-C-means and Advanced Linear Discriminant Analysis

Neema. H.N
Research Scholar, Dept of CA, CS & IT, Karpagam Academy of Higher Education, Coimbatore-641021, India.
Dr. N.V. Balaji
Professor & Director, Centre for Continuing Professional Development, Karpagam Academy of Higher Education, Coimbatore-641021, India.

ABSTRACT:

Attention Deficit Hyperactivity Disorder (ADHD) is one of the most prevalent neurodevelopmental disorders among children worldwide. Conventional diagnosis is primarily based on behavioral and clinical symptom evaluation, which may introduce subjectivity and reduce diagnostic reliability. Although Magnetic Resonance Imaging (MRI) has shown promise in identifying structural brain abnormalities linked to ADHD, existing computational approaches frequently encounter challenges such as high-dimensional feature spaces, inefficient segmentation, suboptimal feature discrimination, classifier overfitting, and limited generalization across heterogeneous datasets. To overcome these limitations, this research proposes an integrated FCM–ALDA framework designed to enhance segmentation accuracy and classification robustness. MRI data obtained from the ADHD-200 Consortium are utilized for model development and validation. The proposed methodology initially performs binary classification to distinguish ADHD subjects from typically developing controls. Subsequently, confirmed ADHD cases are further categorized into three clinical subtypes: ADHD-Inattentive (ADHD-I), ADHD-Hyperactive/Impulsive (ADHD-HI), and ADHD-Combined (ADHD-C). Feature extraction is centered on the Caudate Nucleus, a region critically associated with attention regulation and executive functioning. The Fuzzy C-Means (FCM) clustering algorithm is employed to segment MRI images and extract texture-, intensity-, and shape-based dynamic features, forming the Caudate Nucleus Dataset (CNDS). These features are then classified using Advanced Linear Discriminant Analysis (ALDA) to maximize inter-class separability while minimizing intra-class variance. Comparative evaluation against K-Nearest Neighbor (KNN) and Binary-Coded Genetic Algorithm optimized Extreme Learning Machine (BCGA-ELM) demonstrates that the proposed model achieves superior Accuracy, Sensitivity, and Specificity, confirming its effectiveness for MRI-based ADHD subtype classification.

Keywords: *Attention Deficit Hyperactivity Disorder;* Magnetic Resonance Imaging*; Fuzzy C-Means Clustering; Advanced Linear Discriminant Analysis;* Caudate Nucleus*; ADHD Subtype Classification*

1. INTRODUCTION

ADHD is a highly prevalent neurodevelopmental condition affecting approximately 4–9% of children worldwide, imposing substantial socioeconomic and healthcare burdens [1]. Clinically, ADHD is characterized by persistent patterns of inattention, hyperactivity, and impulsivity that significantly impair academic performance, social functioning, and adaptive behavior. Diagnostic practice is primarily symptom-driven, relying on caregiver reports, behavioral rating scales, and clinical interviews. Based on symptom predominance, ADHD is categorized into three principal subtypes: predominantly inattentive (ADHD-I), predominantly hyperactive-impulsive (ADHD-HI), and combined presentation (ADHD-C) [2]. Current intervention strategies include pharmacotherapy, behavioral therapy, and cognitive training programs, often implemented in multimodal treatment plans [3]. From a neurobiological perspective, ADHD has been strongly associated with genetic predisposition and dysregulation of catecholaminergic neurotransmission, particularly involving dopamine pathways [4]. Neurochemical evidence suggests altered dopamine transporter density within striatal regions, especially in right-lateralized circuits, which are implicated in attention control and reward processing [5]. However, the phenotypic heterogeneity observed in ADHD suggests that multiple interacting neural circuits contribute to symptom manifestation. Understanding structural and functional alterations at the brain-network level is therefore essential for advancing individualized therapeutic strategies and biomarker-driven diagnosis [6].

Neuroimaging has emerged as a promising tool to investigate ADHD-related brain abnormalities. Large-scale collaborative initiatives such as the ADHD-200 Consortium were established to accelerate biomarker discovery by integrating demographic, structural MRI (s-MRI), and resting-state functional MRI (rs-fMRI) datasets [7]. This initiative was supported by data-sharing platforms including the Functional Connectomes Project and the International Neuroimaging Data-sharing Initiative (INDI), facilitating access to large, multisite datasets comprising over 1000 children and adolescents diagnosed with ADHD and Typically Developing (TD) controls. Such repositories enable reproducible computational experimentation and cross-site validation. Despite these advancements, challenges remain in translating neuroimaging findings into clinically reliable diagnostic systems. Many studies lack independent replication cohorts, limiting generalizability and robustness at the individual-subject level [8]. In recent years, Machine Learning (ML) methodologies have been widely adopted for disease classification using neuroimaging data. Applications span neurological and psychiatric conditions, including Alzheimer's disease, schizophrenia, and autism spectrum disorder. These approaches employ diverse feature extraction techniques and classifiers; however, methodological heterogeneity and small sample sizes often constrain model stability [9]. Even though larger datasets such as ADHD-200 have improved statistical power, classification performance still depends heavily on effective feature representation and discriminative modeling [10].

The present study addresses these limitations by focusing on region-specific structural biomarkers derived from MRI, particularly the Caudate Nucleus (CN), a critical component of the fronto-striatal circuitry associated with executive control and attentional regulation. Given the overlapping structural patterns observed across ADHD subtypes, conventional hard clustering methods may inadequately capture subtle inter-class variability. Therefore, FCM clustering is adopted to enable soft partitioning of MRI-derived feature spaces, allowing data points to belong to multiple clusters with varying membership degrees. This enhances segmentation accuracy and preserves structural ambiguity inherent in neuroimaging data. Subsequently, an ALDA framework is employed for classification. Unlike conventional LDA, which utilizes all labeled samples uniformly, ALDA incorporates confidently predicted unlabeled samples to refine class boundaries iteratively. This hybrid discriminative approach improves between-class separability while minimizing intra-class variance, thereby strengthening subtype discrimination among ADHD-I, ADHD-HI, and ADHD-C.

Problem Statement: Despite significant progress in neuroimaging and computational intelligence, an objective ADHD diagnosis remains a challenging task. Current clinical practice is predominantly symptom-based, introducing subjectivity and inter-rater variability. Existing MRI-based classification frameworks often suffer from high-dimensional feature representations, redundancy, and inadequate feature selection strategies, which reduce discriminative power. Conventional hard clustering methods fail to effectively model overlapping structural characteristics present in brain MRI data. Moreover, traditional LDA assumes strict linear separability and complete label availability, limiting its adaptability to semi-structured neuroimaging datasets. Many prior studies also report limited generalization due to small sample sizes or heterogeneous multisite data. Therefore, a robust, region-specific, and computationally efficient framework is required to enhance segmentation accuracy and improve ADHD subtype classification performance.

MSW MANAGEMENT -Multidisciplinary, Scientific Work and Management Journal
ISSN: 1053-7899
Vol. 36 Issue 1, 2026, Pages: 1862-1871

Paper Contributions: This study proposes a technically robust MRI-based classification framework centered on structural biomarkers derived from the Caudate Nucleus, a key component of the fronto-striatal circuitry implicated in attentional control.

- First, FCM clustering is implemented to perform soft segmentation, enabling effective handling of overlapping feature distributions in MRI data.
- Second, a structured CNDS is constructed by extracting discriminative Texture, Intensity, and Shape-based features.
- Third, an ALDA model is introduced to enhance inter-class separability while minimizing intra-class variance.
- Unlike conventional LDA, the proposed ALDA incorporates confidently predicted unlabeled samples to refine classification boundaries iteratively. The framework supports both binary ADHD detection and subsequent subtype stratification (ADHD-I, ADHD-HI, ADHD-C).
- Comprehensive validation is conducted using multisite data from the ADHD-200 Consortium, demonstrating improved robustness and generalization compared to conventional ML baselines.

Paper Organization: The remainder of this paper is structured as follows. Section 2 presents a comprehensive review of recent literature related to MRI-based ADHD classification and ML methodologies. Section 3 describes the proposed FCM–ALDA framework, detailing preprocessing procedures, feature extraction mechanisms, clustering strategy, and classification architecture. Section 4 discusses experimental results, performance metrics, and comparative analysis with baseline models. Finally, Section 5 concludes the paper and outlines potential directions for future research in neuroimaging-driven ADHD diagnosis.

2. RELATED WORKS

In [11], the authors analyzed MRI head motion patterns across typical development and ADHD populations, revealing significant differences that influence functional and structural imaging quality. They found that motion artifacts vary systematically with age and diagnostic status, with ADHD subjects exhibiting characteristic motion patterns that can confound neuroimaging analyses. These motion dynamics have important implications for preprocessing pipelines and classifier performance, as uncorrected motion can bias extracted features and lead to spurious classification results. By quantifying motion effects, the work establishes the need for adaptive correction strategies and robust feature extraction algorithms that explicitly account for subject movement, particularly in pediatric imaging datasets. It underscores that methodological considerations beyond classification algorithms themselves are critical for accurate ADHD MRI models.

In [12], the authors proposed a state-of-the-art deep learning framework for ADHD classification using resting-state functional MRI (rs-fMRI). The study implements a ConvLSTM architecture with targeted data augmentation (temporal jittering and regulated Gaussian noise) to address data scarcity and class imbalance, achieving high classification performance (F1-score = 0.89, accuracy = 0.90, AUC = 0.96) on the ADHD-200 dataset. Additionally, model generalizability was validated on independent external cohorts, obtaining perfect specificity and precision with balanced accuracy of 83.3% as a rare demonstration of cross-cohort validation. Crucially, the integration of Grad-CAM explainability highlights brain regions that contribute most to diagnosis, improving interpretability, a major barrier in clinical AI adoption. Despite promising results, the study notes that larger multi-center validation is required to substantiate translational reliability. This research thus exemplifies an interpretable and reproducible deep learning pipeline tailored for neuroimaging-based ADHD detection.

In [13], the authors introduced interpretable ML models using clinical assessment data, including ratings from parents, self-reports, and neuropsychological measures, demonstrating high diagnostic accuracy (AUC ≈ 0.886–0.906) for distinguishing ADHD from controls. Nested cross-validation frameworks ensured robust performance estimates, and feature importance analysis consistently highlighted social problems, executive dysfunction, and self-regulation measures as top predictors across models. Although not MRI-based, this work underscores the importance of interpretability in model outputs, suggesting that models that integrate behavioral, clinical, and potentially imaging data may support more objective and explainable diagnoses. Its focus on clinically practical predictors provides a complementary perspective to purely imaging-based models, advocating for hybrid multimodal frameworks.

In [14], the authors examined ML techniques used for MRI and/or EEG-based ADHD detection, following PRISMA 2020 guidelines and evaluating 87 studies. The review highlighted that the widely used ADHD-200 dataset remains the standard, but studies vary substantially in algorithm choice, feature extraction, and evaluation metrics. It also emphasized methodological biases and insufficient external validation, which impede comparability and clinical translation. The authors pointed out that multimodal models combining imaging and non-imaging data achieve more robust performance and provide a future direction for generalizable frameworks. Importantly, the review identifies a need for more harmonized protocols and unbiased evaluation pipelines in future ADHD diagnostic research to achieve consensus performance benchmarks.

In [15], the authors applied advanced population modeling to large multisite structural MRI data to explore ADHD heterogeneity within and across neurodevelopmental disorders. Using centile scores of cortical thickness, surface area, and grey matter volume, the authors applied a semi-supervised ML algorithm (HYDRA) to identify distinct neuroanatomical subgroups in autism and ADHD compared to controls. The identified subgroups exhibited opposite structural alterations, suggesting distinct morphological phenotypes that may relate to clinical variability and treatment response differences. However, the results were found to be highly sensitive to feature selection and clustering methodology, emphasizing the need for careful methodological reporting. This work highlights the potential for unsupervised and semi-supervised MRI analysis to move beyond traditional diagnostic labels and toward biologically informed subtyping, demonstrating structural MRI's capacity to reveal latent heterogeneity within ADHD presentations.

Research Gap: Despite advancements in MRI-based ADHD classification techniques, key gaps remain. First, the external generalizability of deep learning models on independent cohorts remains under-validated, limiting clinical adoption. Second, heterogeneity in ADHD subtypes and structural phenotypes has not yet been effectively translated into diagnostic frameworks that clinicians can interpret and apply. Third, many studies lack harmonized preprocessing and evaluation standards, which hinders the comparability and reproducibility of results. Fourth, preprocessing challenges, such as MRI motion artifacts, continue to bias feature extraction and classification outcomes. Fifth, purely imaging-based models often lack interpretability and clinical explainability, reducing trust among practitioners. Finally, multimodal integration of imaging with behavioral, genetic, or clinical data is still underexplored, suggesting the need for holistic, biologically grounded diagnostic models.

3. METHODOLOGIES

In the present study, structural MRI datasets obtained from the ADHD-200 Consortium were utilized to develop and validate the proposed classification framework for identifying ADHD in children. The methodological pipeline encompasses data acquisition, preprocessing, region-of-interest segmentation, feature extraction using FCM, and classification through ALDA. A systematic representation of the proposed computational workflow is illustrated in Figure 1, detailing each stage from raw MRI input to final ADHD subtype classification.

MSW MANAGEMENT -Multidisciplinary, Scientific Work and Management Journal
ISSN: 1053-7899
Vol. 36 Issue 1, 2026, Pages: 1862-1871

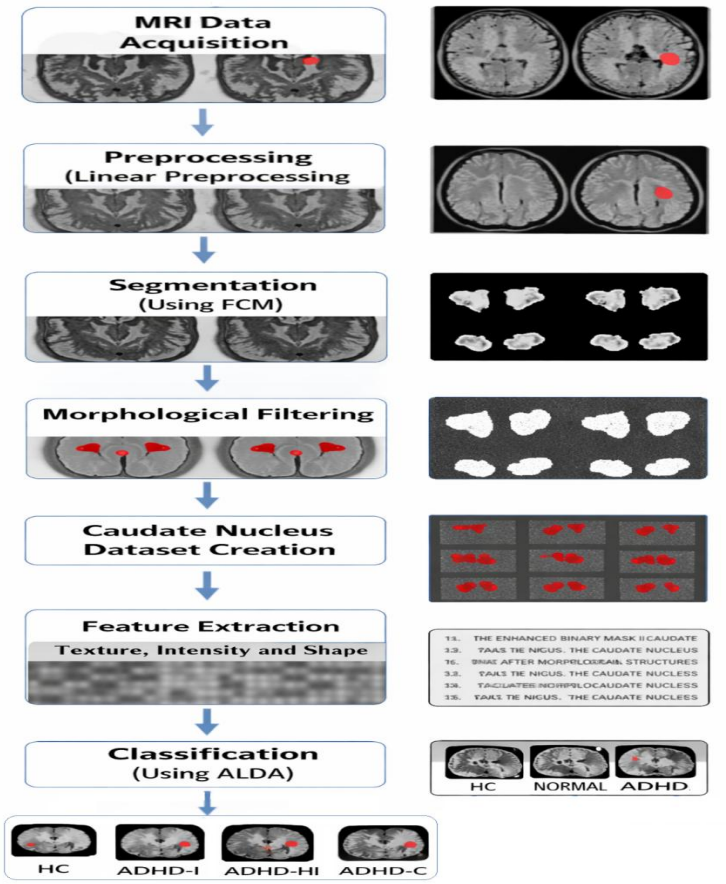

Figure 1: Proposed FCM-ALDA Work Flow

3.1 MRI Data Acquisition

sMRI datasets used in this study were obtained from the publicly accessible ADHD-200 Consortium repository. The cohort comprised children and adolescents aged between 3 and 15 years who were clinically diagnosed with ADHD. Neuroimaging data were acquired using a 1.5-Tesla MRI scanner to ensure adequate spatial resolution and tissue contrast for structural analysis. T2-weighted (T2W) brain images were captured in the axial plane using standardized acquisition parameters: 23 contiguous slices with repetition time (TR) = 5400 ms, echo time (TE) = 97 ms, inversion time (TI) = 1000 ms, flip angle = 7°, excitation (nutation) angle = 90°, slice thickness = 3 mm, and an inter-slice gap of 0.3 mm. The voxel resolution was maintained at 1.0 × 1.0 × 1.0 mm³, with a field of view (FOV) of 300 mm and an image matrix size of 256 × 256. These parameters were selected to optimize grey matter–white matter contrast and enable reliable morphometric feature extraction. To minimize motion artifacts, foam padding was placed within the head coil to stabilize head orientation during scanning. High-resolution visualization of internal brain structures was facilitated through intensity enhancement and appropriate image normalization procedures. The acquired MRI volumes were subsequently converted into standard image formats (e.g., BMP and JPEG) for preprocessing and computational analysis. Representative MRI brain images used as input to the proposed framework are illustrated in Figure 2.

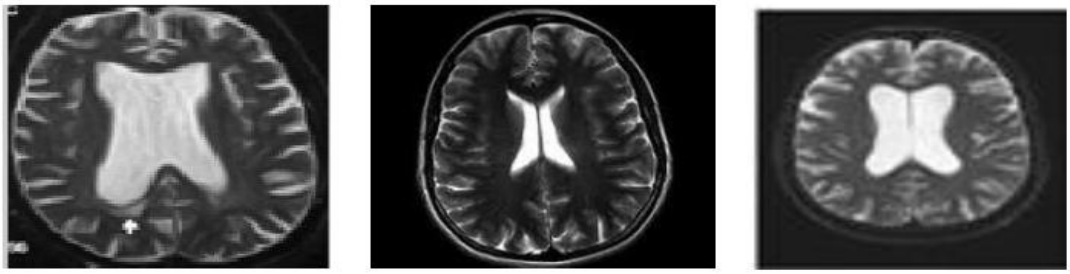

Figure 2: Sample MRI Brain Images

3.2 Preprocessing using Linear Preprocessing

Preprocessing constitutes a critical stage in medical image analysis, particularly for improving feature reliability and segmentation accuracy. Raw MRI images frequently contain illumination inhomogeneities, shadowing artifacts, and intensity non-uniformities arising from scanner variability and acquisition conditions. To mitigate these inconsistencies and standardize the intensity distribution across samples, a linear preprocessing technique based on intensity normalization was employed. Linear preprocessing performs contrast stretching by transforming the original pixel intensity range into a normalized interval. This operation enhances global contrast while preserving structural information relevant for downstream segmentation and feature extraction. Mathematically, the normalized pixel intensity "I_N" is computed as per Equation (1):

$$I_N = \frac{(I-Min)}{(Max-Min)} * (Max_N - Min_N) + Min_N \quad (1)$$

Where "I" denotes the original pixel intensity value, "Min" and "Max" represent the minimum and maximum intensity values in the original image, "Min_N" and "Max_N" correspond to the desired minimum and maximum intensity values after normalization, and

MSW MANAGEMENT -Multidisciplinary, Scientific Work and Management Journal
ISSN: 1053-7899
Vol. 36 Issue 1, 2026, Pages: 1862-1871

"I_N" is the normalized pixel intensity value. In this study, intensity values were linearly rescaled to the range [0, 1] to ensure numerical stability and uniform dynamic range across MRI samples. This contrast enhancement technique effectively stretches the histogram such that the lowest intensity is mapped to the minimum normalized value and the highest intensity is mapped to the maximum normalized value. Consequently, grey-level distributions become more distinguishable, facilitating improved segmentation performance using FCM and enhancing discriminative feature extraction for subsequent classification.

3.3 Segmentation using FCM

Image segmentation plays a pivotal role in isolating anatomically relevant regions from structural MRI scans for quantitative analysis. In this study, segmentation is performed using the FCM clustering algorithm, an unsupervised soft-partitioning technique particularly suitable for medical imaging applications. Unlike hard clustering methods, where each pixel is assigned exclusively to a single cluster, FCM assigns each pixel a membership value within the interval [0,1], enabling partial association with multiple clusters. This property is especially advantageous in brain MRI analysis, where tissue boundaries are often ambiguous, and intensity distributions overlap. The FCM algorithm partitions the dataset such that intra-cluster similarity is maximized while inter-cluster similarity is minimized. In the present framework, pixel intensities exhibit stronger correlations within homogeneous tissue regions and weaker correlations across distinct anatomical structures. Fuzzy partitioning is achieved by iteratively optimizing cluster centers to minimize an objective function, allowing effective modeling of overlapping regions and boundary uncertainties. This soft segmentation strategy is particularly appropriate for isolating the Caudate Nucleus (CN), where structural variations may not exhibit sharply defined edges.

FCM Algorithmic Procedure:

Let the dataset be represented as "X = {x_1, x_2, x_3, …, x_n}", where 'n' denotes the number of data samples to be partitioned into 'C' clusters. The FCM algorithm follows these steps:

(i) Select the input preprocessed MRI image and determine its dimensions.
(ii) Define the number of clusters 'C' and the maximum iteration limit.
(iii) Convert the preprocessed image into a feature vector space.
(iv) Initialize cluster centers "V_j" randomly, where "j = 1, 2, ..., C".
(v) Compute fuzzy membership values "μ_{ij}" for each data point with respect to cluster centers as defined in Equation (2):

$$\mu_{ij} = \frac{1}{\sum_{k=1}^{C}\left(\frac{||x_i - v_j||}{||x_i - v_k||}\right)^{\frac{2}{m-1}}} \quad (2)$$

(vi) Update cluster centers as defined in Equation (3):

$$v_j = \frac{\sum_{i=1}^{n}(\mu_{ij})^m x_i}{\sum_{i=1}^{n}(\mu_{ij})^m} \quad (3)$$

(vii) Repeat steps (v) and (vi) until convergence, i.e., when the change in the objective function 'J' falls below a predefined threshold. The objective function minimized by FCM as per Equation (4):

$$J = \sum_{i=1}^{n}\sum_{j=1}^{C}(\mu_{ij})^m \, ||x_i - v_j||^2 \quad (4)$$

Where 'n' is the total number of data points, 'C' is the number of clusters, 'm' is the fuzziness index (controls the degree of cluster overlap), "μ_{ij}" is membership of the "i^{th}" data point to the "j^{th}" cluster, "v_j" is the center of the "j^{th}" cluster, and "$||x_i - v_j||$" is the Euclidean distance between data point "x_i" and cluster center "v_j". Figure 3 illustrates the segmentation output of the CN region using the FCM approach. The method provides precise delineation of the CN from surrounding brain tissues, producing a refined and structurally coherent representation suitable for subsequent feature extraction and classification stages.

Figure 3: Segmentation Output by FCM

3.4 Morphological Filtering

Following segmentation, minor artifacts and spurious pixel clusters may remain in the segmented output due to intensity overlap or suboptimal threshold selection. These undesired components often do not belong to the Caudate Nucleus (CN) and can adversely affect subsequent feature extraction. Therefore, a post-segmentation refinement step using Morphological Filtering (MF) is applied to enhance structural consistency and remove irrelevant regions. Morphological operations are nonlinear image processing techniques based on the geometrical structure of objects within an image. Fundamental morphological transformations include dilation, erosion, opening, and closing. These operations rely on a predefined structuring element that determines how pixel neighborhoods are examined and modified. In this study, the morphological opening operation is employed to eliminate small foreground artifacts while preserving the principal anatomical structure of interest. Morphological opening is defined as the sequential application of erosion followed by dilation. Mathematically, the opening of an image 'f' by a structuring element 's' is expressed in Equation (5):

$$f \; o \; s = (f \; \Theta \; s) \oplus s \quad (5)$$

Where 'Θ' denotes erosion, '⊕' denotes dilation, and "$f \; o \; s$" represents the opened image. Erosion removes small, isolated foreground components and shrinks object boundaries, while dilation restores the primary object's size without reintroducing eliminated noise. As a result, minor foreground regions that deviate from the CN structure are effectively removed, whereas larger and structurally significant regions remain intact. In the proposed framework, FCM segmentation initially isolates candidate CN regions from MRI brain images. Subsequently, the MF opening operation refines the segmentation output by retaining only the anatomically consistent CN structure and suppressing extraneous elements. The resulting output, illustrated in Figure 4, demonstrates an improved and structurally coherent representation of the CN, suitable for robust feature extraction and classification.

MSW MANAGEMENT -Multidisciplinary, Scientific Work and Management Journal
ISSN: 1053-7899
Vol. 36 Issue 1, 2026, Pages: 1862-1871

Figure 4: Morphological Filtering

3.5 Caudate Nucleus Dataset

In the proposed framework, the extraction of the CN is accomplished through a sequential pipeline comprising linear preprocessing, intensity enhancement, FCM segmentation, and morphological filtering. These operations are applied to the original axial T2-weighted structural MRI brain images to ensure accurate delineation of the CN region while suppressing irrelevant anatomical structures and background artifacts. Following segmentation and refinement, the isolated CN regions are systematically stored and organized into a structured repository referred to as the CNDS. Each entry in the CNDS corresponds to a segmented CN image associated with its respective subject label (ADHD or control), thereby facilitating supervised classification and subtype analysis. The dataset serves as the primary input for subsequent feature extraction, where texture-, intensity-, and shape-based attributes are computed for discriminative modeling. By isolating the CN before feature computation, the CNDS reduces dimensional redundancy and enhances the signal-to-noise ratio in the learning process. This region-specific dataset design supports more focused analysis of structural biomarkers associated with ADHD-related neuroanatomical variations. Representative examples of extracted CN images alongside their corresponding source MRI scans are illustrated in Figure 5, demonstrating the effectiveness of the segmentation and refinement pipeline.

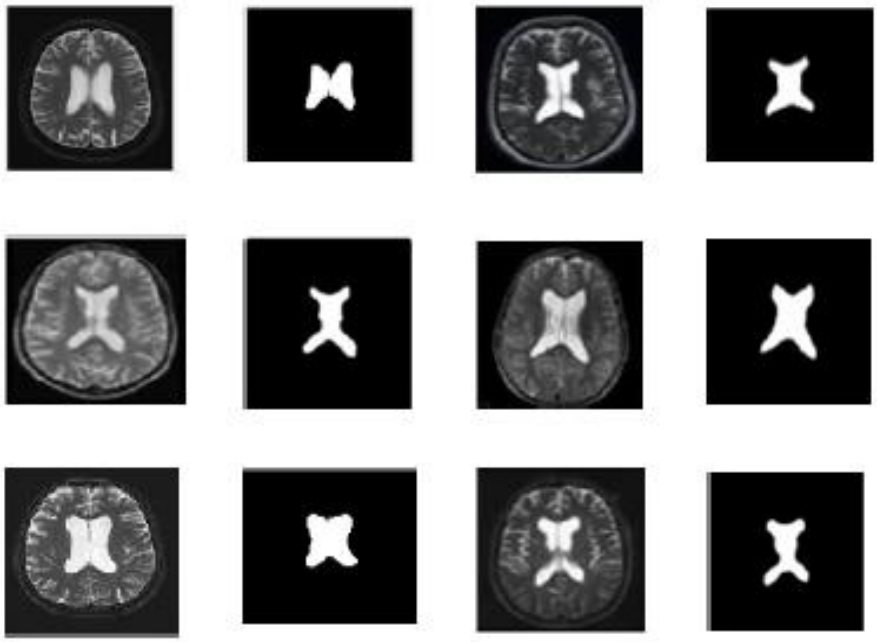

Figure 5: CNDS Images

3.6 Feature Extraction

Following the construction of the CNDS, quantitative feature extraction is performed to characterize structural and textural variations in the CN. The objective of this stage is to transform segmented CN images into discriminative numerical descriptors suitable for statistical analysis and ML classification. Three principal feature categories are considered: texture, intensity, and shape-based attributes.

- **Texture features** are computed using second-order statistical measures derived from the Gray-Level Co-occurrence Matrix (GLCM). The extracted parameters include Contrast, Energy, Homogeneity, and Correlation. Contrast quantifies local intensity variations, Energy measures textural uniformity, Homogeneity evaluates the closeness of element distribution to the diagonal of the GLCM, and Correlation assesses the linear dependency of gray levels in neighboring pixels. These metrics effectively capture microstructural alterations in CN tissue patterns.
- **Intensity-based features** describe first-order statistical properties of pixel distributions within the segmented region. The Mean represents the average gray-level intensity, the Standard Deviation measures dispersion around the mean, and the variance reflects overall intensity variability. These features provide insights into tissue density variations and structural heterogeneity.
- **Shape features** quantify geometric properties of the segmented CN region. Area represents the total number of pixels constituting the CN in a slice, while Volume is estimated by integrating area measurements across slices, considering slice thickness and inter-slice spacing. These parameters capture morphological differences potentially associated with ADHD-related neurodevelopmental changes.

The extracted texture, intensity, and shape features from both severe ADHD and healthy control groups are systematically analyzed and compared in the Results and Discussion section to evaluate their discriminative significance and clinical relevance.

MSW MANAGEMENT -Multidisciplinary, Scientific Work and Management Journal
ISSN: 1053-7899
Vol. 36 Issue 1, 2026, Pages: 1862-1871

3.7 Classification using ALDA

To enhance discriminative performance under limited labeled data, an ALDA framework incorporating unlabeled samples is proposed. Unlike conventional LDA, which relies exclusively on labeled observations, the proposed approach selectively integrates high-confidence unlabeled data into the training process. This semi-supervised extension improves class separability while preserving statistical reliability. Although predicted class labels for unlabeled samples may not be perfectly accurate, incorporating confidence estimation mitigates the risk of distributional distortion. To estimate both class labels and their associated certainty, a modified Linear Neighborhood Propagation (LNP) algorithm is employed in ALDA. LNP is a transductive semi-supervised learning method that infers labels for unlabeled samples by exploiting structural relationships with labeled data in feature space. Graph-based learning methods operate under the assumption that neighboring data points are likely to share similar class labels. Accordingly, LNP first constructs a weighted adjacency graph, where each data point is represented as a weighted linear combination of its nearest neighbors (similar to locally linear embedding principles). Label information is then propagated across the graph from labeled to unlabeled nodes.

(i) Dataset Representation: Let the dataset be represented as "$X \cup U$", where:

- X = [x_1, …, x_n] denotes labeled data belonging to one of 'r' classes
- U = [x_{n+1}, ..., x_{n+u}] denotes unlabeled data

For each unlabeled data point, LNP produces a score vector:

$$[t_{i1}, t_{i2}, ..., t_{ik}]$$

Where "t_{ik}" represents the likelihood of belonging to class 'k'. The sample is assigned to the class with the maximum "t_{ik}" value:

$$\hat{y}_i = argmax_k(t_{ik})$$

A certainty metric is computed based on the distribution of the "t_{ik}" values. When the dominant "t_{ik}" significantly exceeds the others, the certainty approaches 1. Only unlabeled samples with sufficiently high certainty are incorporated into the extended labeled dataset. Equation (6) defines that after augmentation, the expanded labeled dataset becomes:

$$X^* = [x_1, \dots x_{n^*}] \quad (6)$$

The original labeled samples retain certainty value "$b_i = 1$", while the appended unlabeled samples are assigned certainty values "$0 < b_i < 1$". These certainty measures are embedded into the similarity and penalty matrices during discriminant computation.

(ii) Similarity and Penalty Matrix Construction: If two samples "x_i" and "x_j" belong to class 'k', the similarity matrix element "s_{ij}" is defined as in Equation (7):

$$s_{ij} = \frac{b_i b_j}{n_k} \quad (7)$$

Where "n_k" is the number of samples in class 'k'. Otherwise, if "x_i" and "x_j" belong to different classes, the penalty matrix element "p_{ij}" is defined as in Equation (8):

$$p_{ij} = \frac{b_i b_j}{n^*} \quad (8)$$

Where "n*" is the total number of samples in "X*". The diagonal matrices "Ds" and 'Dp" are constructed such that their "i^{th}" diagonal entries are:

$$D_s(i,i) = \sum_j s_{ij}$$

$$D_p(i,i) = \sum_j p_{ij}$$

(iii) ALDA Projection Formulation: The optimal projection directions are obtained by solving the generalized eigenvalue problem it mathematically formulated as defined in Equation (9):

$$X^*(D_s - S){X^*}^T W = \lambda X^*\big(D_p - P\big){X^*}^T W \quad (9)$$

Where "S = [s_{ij}]" is the similarity matrix, "P = [p_{ij}]" is the penalty matrix, and 'λ' denotes eigenvalues. The eigenvectors corresponding to the largest eigenvalues define the discriminative subspace for classification. When unlabeled data are excluded (i.e., (b_i = 1) for all samples), the formulation reduces to classical LDA as defined in Equation (10):

$$S_b W = \lambda\, S_w W \quad (10)$$

Where "S_b" and "S_w" denote the between-class and within-class scatter matrices, respectively. By integrating high-confidence unlabeled samples, ALDA improves within-class compactness and between-class separability while maintaining robustness against misclassification noise. This approach is particularly effective in medical imaging scenarios where labeled datasets are limited but unlabeled samples are abundant.

4. RESULTS AND DISCUSSIONS

4.1 Dataset Description: The proposed ALDA framework was evaluated using structural MRI data from the ADHD-200 Global Competition Dataset (ADHD Consortium Dataset)**.** The dataset consists of T2-weighted axial brain MRI scans of children aged 3–15 years, clinically categorized into four groups: Healthy Control (HC), ADHD–Inattentive (ADHD-I), ADHD–Hyperactive/Impulsive (ADHD-HI), and ADHD–Combined (ADHD-C). All MRI scans were preprocessed and subjected to FCM segmentation followed by morphological filtering to extract the Caudate Nucleus (CN) region. The segmented CN images were compiled into the CNDS. From each CN region, texture (Contrast, Energy, Homogeneity, Correlation), intensity (Mean, Standard Deviation, Variance), and shape (Area, Volume) features were extracted to form the final feature matrix used for four-class classification (HC vs. ADHD-I vs. ADHD-HI vs. ADHD-C).

4.2 Tools and Experimental Setup: All experiments were conducted in the MATLAB (MathWorks Inc., USA) environment. Image preprocessing, FCM-based segmentation, morphological filtering, and feature extraction were implemented using MATLAB's Image Processing Toolbox. The proposed ALDA classifier, including LNP, certainty estimation, similarity–penalty matrix construction, and generalized eigenvalue computation, was developed using MATLAB's matrix computation and linear algebra functionalities. Classification performance was evaluated using confusion-matrix-based performance metrics.

4.3 Performance Metrics: To evaluate the effectiveness of the proposed ALDA model, performance was assessed using confusion-matrix-based statistical measures. These metrics quantify the ability of the classifier to correctly distinguish between Healthy Control (HC) subjects and ADHD subtypes (ADHD-I, ADHD-HI, ADHD-C). For comparative evaluation, two established ML models were implemented as baseline classifiers:

- **KNN**: A distance-based non-parametric classifier that assigns class labels based on the majority vote of the nearest neighbors in feature space.

MSW MANAGEMENT -Multidisciplinary, Scientific Work and Management Journal
ISSN: 1053-7899
Vol. 36 Issue 1, 2026, Pages: 1862-1871

- **BCGA-ELM**: A hybrid model in which an ELM is optimized using a BCGA to enhance weight selection and generalization performance.

KNN represents a classical instance-based learning approach, while BCGA-ELM represents an evolutionary optimized neural framework. The proposed ALDA method is compared against these models to demonstrate improvements in discriminative learning under semi-supervised conditions.

4.3.1 Accuracy: Accuracy measures the proportion of correctly classified samples to the total number of evaluated samples. It reflects the overall correctness of a classification model across all classes. Accuracy is formulated as per Equation (11):

$$Accuracy = \frac{Number\ of\ Correct\ Predictions}{Total\ Number\ of\ Samples} \quad (11)$$

For multi-class classification, the Accuracy is formulated as per Equation (12):

$$Accuracy = \frac{\sum_{i=1}^{C} TP_i}{N} \quad (12)$$

Where "TP_i" denotes True Positives of class 'i', 'C' denotes the total number of classes, and 'N' denotes the total number of samples. In this work, accuracy is computed class-wise to evaluate the discriminative capability of the classifiers in distinguishing Healthy Controls (HC) and ADHD subtypes (ADHD-I, ADHD-HI, ADHD-C). The proposed FCM-ALDA model is compared with KNN and BCGA-ELM to assess classification robustness and subtype sensitivity.

Table 1: Class-wise Accuracy Comparison (%)

Types	KNN (%)	BCGA-ELM (%)	FCM-ALDA (%)
HC	94	97	98
ADHD-I	86	92	96
ADHD-HI	90	94	97
ADHD-C	91	96	98

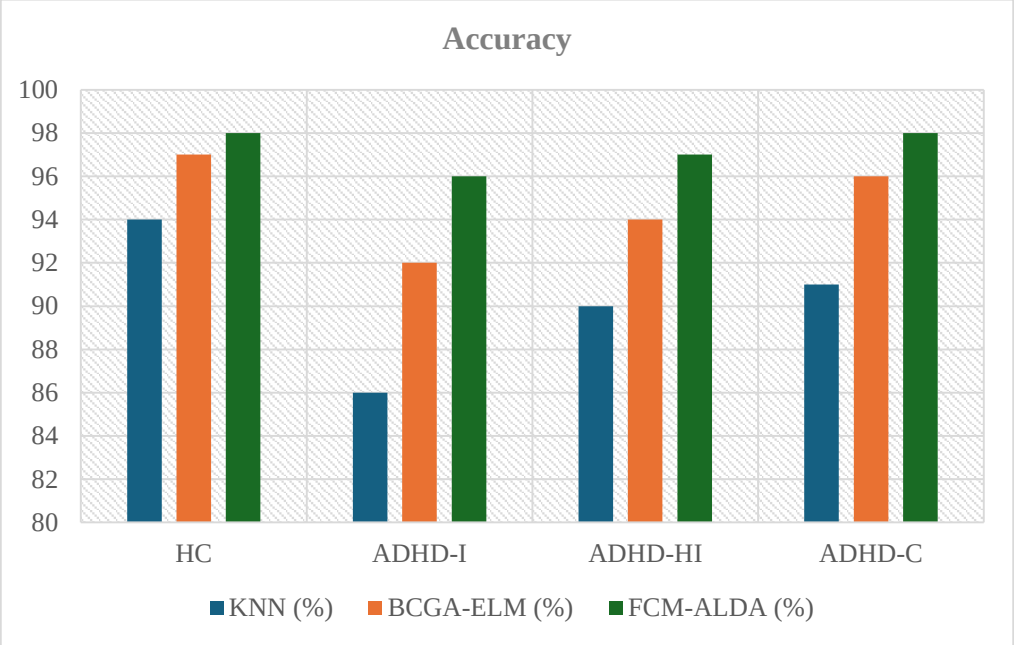

Figure 6: Accuracy Comparison

Table 1 and Figure 6 results demonstrate that the proposed FCM-ALDA model achieves superior classification accuracy across all categories. KNN exhibits comparatively lower performance, particularly for ADHD-I (86%) and ADHD-C (91%), indicating limitations in handling complex intra-class feature variations using distance-based learning alone. BCGA-ELM improves accuracy through evolutionary optimization of network parameters; however, its purely supervised structure restricts its adaptability to subtle feature distributions. In contrast, FCM-ALDA consistently attains the highest accuracy values, notably achieving 96% for ADHD-I and 98% for ADHD-C. The improvement is particularly significant in ADHD-I, which is clinically more challenging due to less pronounced hyperactivity markers. The integration of certainty-weighted unlabeled samples and discriminant subspace projection enhances class compactness and separability. These findings confirm that the proposed semi-supervised framework effectively strengthens discriminative learning under limited labeled data conditions.

4.3.2 Sensitivity: Sensitivity, also known as Recall or True Positive Rate (TPR), measures the proportion of actual positive samples that are correctly identified by the classifier. In clinical classification problems such as ADHD subtype detection, sensitivity is crucial because it reflects the ability of the model to correctly detect affected individuals while minimizing false negatives. A higher sensitivity value indicates improved detection capability and reduced risk of misdiagnosis. For each class 'i', the Sensitivity is formulated as per Equation (13):

$$Sensitivity = \frac{TP_i}{TP_i + FN_i} \quad (13)$$

Where "TP_i" denotes True Positives for class 'i', and "FN_i" denotes False Negatives for class 'i'. In this study, sensitivity evaluates how effectively each classifier detects Healthy Controls (HC) and ADHD subtypes (ADHD-I, ADHD-HI, ADHD-C). Since missing ADHD cases can adversely affect clinical assessment, sensitivity serves as a critical diagnostic reliability metric.

MSW MANAGEMENT -Multidisciplinary, Scientific Work and Management Journal
ISSN: 1053-7899
Vol. 36 Issue 1, 2026, Pages: 1862-1871

Table 2: Class-wise Sensitivity Comparison (%)

Types	KNN (%)	BCGA-ELM (%)	FCM-ALDA (%)
HC	92	96	97
ADHD-I	84	90	95
ADHD-HI	88	92	96
ADHD-C	89	94	97

Table 2 and Figure 7 results indicate that the proposed FCM-ALDA model achieves superior true positive detection across all clinical categories. KNN demonstrates comparatively lower sensitivity, particularly for ADHD-I (84%), suggesting higher false negative occurrences in detecting inattentive subtype cases. BCGA-ELM improves detection performance through optimized learning parameters; however, its purely supervised framework limits robustness under subtle subtype variations. The proposed FCM-ALDA achieves the highest sensitivity in all classes, notably 95% for ADHD-I and 97% for ADHD-C, indicating enhanced recognition of clinically heterogeneous subtypes. The semi-supervised certainty-weighted discriminant learning improves within-class compactness and reduces misclassification. These findings confirm that FCM-ALDA strengthens diagnostic sensitivity while maintaining classification stability across ADHD subtypes.

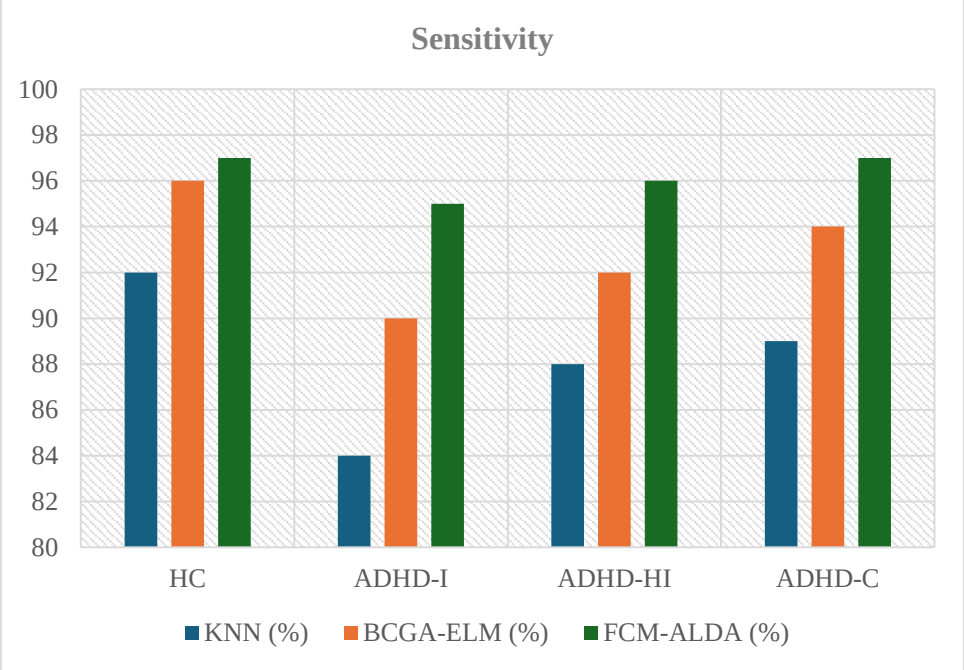

Figure 7: Sensitivity Comparison

4.3.3 Specificity: Specificity, also known as the True Negative Rate (TNR), measures the proportion of actual negative samples that are correctly identified by the classifier. In multi-class medical classification, specificity reflects the ability of the model to correctly reject non-target classes without falsely labeling them as the given class. High specificity is important to prevent false alarms, particularly in distinguishing Healthy Controls from ADHD subtypes and avoiding incorrect subtype assignments. For each class 'i', the Specificity is formulated as per Equation (14):

$$Specificity = \frac{TN_i}{TN_i + FP_i} \quad (14)$$

Where "TN_i" denotes True Negatives for class 'i', "FP_i" denotes False Positives for class 'i'. Specificity is computed independently for each class in the multi-class framework. In this study, specificity evaluates how effectively the classifiers avoid misclassifying samples from other classes as the target class. It complements sensitivity by quantifying the false positive control capability of KNN, BCGA-ELM, and FCM-ALDA in ADHD subtype differentiation.

Table 3: Class-wise Specificity Comparison (%)

Types	KNN (%)	BCGA-ELM (%)	FCM-ALDA (%)
HC	95	98	99
ADHD-I	88	93	97
ADHD-HI	91	95	98
ADHD-C	92	97	99

MSW MANAGEMENT -Multidisciplinary, Scientific Work and Management Journal
ISSN: 1053-7899
Vol. 36 Issue 1, 2026, Pages: 1862-1871

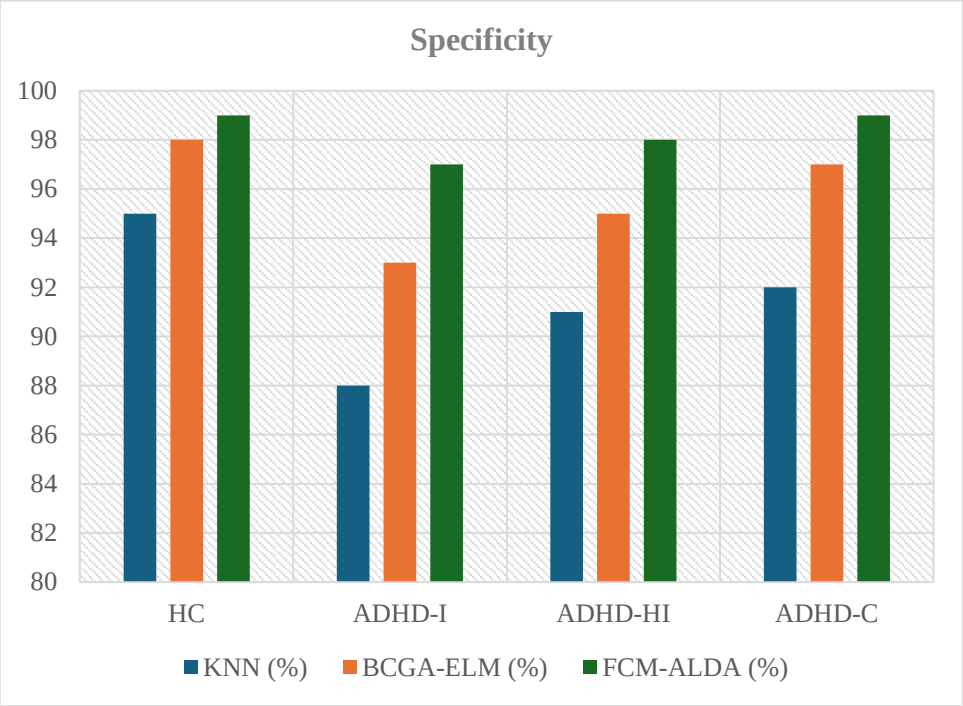

Figure 8: Specificity Comparison

Table 3 and Figure 8 analysis demonstrate that the proposed FCM-ALDA model achieves superior true negative discrimination across all classes. KNN exhibits comparatively lower specificity, particularly in ADHD-I (88%), indicating increased false positive misclassification among closely related subtypes. BCGA-ELM improves negative class rejection through optimized parameter tuning; however, its performance remains lower than that of the proposed method. FCM-ALDA achieves near-perfect specificity values, reaching 99% for HC and ADHD-C classes, reflecting strong separation between clinically overlapping groups. The semi-supervised discriminant projection effectively enhances between-class margin separation, thereby minimizing false subtype assignments. The balanced improvement in both sensitivity and specificity confirms that FCM-ALDA maintains robust diagnostic reliability without overfitting toward positive detection.

4.4 Comparative Discussion

The comparative evaluation of KNN, BCGA-ELM, and the proposed FCM-ALDA model demonstrates consistent and statistically meaningful performance improvements across all evaluation metrics.

- Based on the class-wise accuracy results, FCM-ALDA achieves the highest overall classification performance, particularly in clinically complex subtypes such as ADHD-I and ADHD-C. The improvement in accuracy indicates enhanced discriminative capability and better feature space structuring through certainty-weighted semi-supervised learning.
- Sensitivity analysis further confirms the robustness of the proposed framework. KNN exhibits reduced true positive detection, especially for ADHD-I, suggesting limitations in capturing subtle neuroimaging variations using distance-based classification. BCGA-ELM improves detection capability through evolutionary weight optimization; however, its reliance on fully labeled data restricts adaptability under limited supervision. In contrast, FCM-ALDA consistently achieves superior sensitivity across all categories, indicating effective reduction of false negatives. This is particularly significant in medical classification, where missed ADHD cases can adversely impact clinical decision-making.
- Specificity results demonstrate that FCM-ALDA also maintains strong false positive control. While KNN shows moderate specificity and BCGA-ELM provides incremental improvement, the proposed model achieves the highest true negative rates across all classes. The balanced enhancement of both sensitivity and specificity indicates that FCM-ALDA does not bias the classifier toward over-detection or conservative rejection. Instead, it improves intra-class compactness and maximizes inter-class separability through discriminant subspace projection enriched with high-confidence unlabeled samples.
- Overall, the simultaneous improvement in Accuracy, Sensitivity, and Specificity confirms that the proposed semi-supervised FCM-ALDA framework achieves superior generalization performance compared to conventional instance-based (KNN) and evolutionary neural (BCGA-ELM) models. The results validate its suitability for multi-class ADHD subtype classification using MRI-derived caudate nucleus features, particularly in scenarios with limited labeled medical data.

5. CONCLUSION

This study presented a semi-supervised classification framework for ADHD subtype identification using CN features extracted from axial T2-weighted MRI images. The proposed FCM-ALDA model integrates FCM–based segmentation with an ALDA approach incorporating high-confidence unlabeled samples. Texture, intensity, and shape features were extracted to characterize structural variations associated with Healthy Controls and ADHD subtypes (ADHD-I, ADHD-HI, and ADHD-C). Comparative evaluation against KNN and BCGA-ELM demonstrated that FCM-ALDA consistently achieved superior Accuracy, Sensitivity, and Specificity across all categories. The incorporation of certainty-weighted unlabeled data improved discriminative subspace learning, enhanced intra-class compactness, and maximized inter-class separability. Importantly, the model maintained balanced TP and TN rates, indicating robustness against both FN and FP. The findings confirm that semi-supervised discriminant learning is highly effective in medical imaging scenarios where labeled datasets are limited. Overall, the proposed framework provides a reliable and clinically relevant approach for automated ADHD subtype classification using MRI-derived biomarkers. Future research may explore deep representation learning using Vision Transformers (ViT) or Graph Convolutional Networks (GCN) to further enhance structural feature modeling and subtype discrimination performance.

MSW MANAGEMENT -Multidisciplinary, Scientific Work and Management Journal
ISSN: 1053-7899
Vol. 36 Issue 1, 2026, Pages: 1862-1871

REFERENCES:

1. Johnson, S., Lim, E., Jacoby, P., Faraone, S. V., Su, B. M., Solmi, M., et al. (2025). Prevalence of attention deficit hyperactivity disorder/hyperkinetic disorder of pediatric and adult populations in clinical settings: A systematic review, meta-analysis and meta-regression. Molecular Psychiatry, 31(1), 576–586. https://doi.org/10.1038/s41380-025-03178-8
2. Frodl, T., & Skokauskas, N. (2012). Meta-analysis of structural MRI studies in children and adults with attention deficit hyperactivity disorder indicates treatment effects. Acta Psychiatrica Scandinavica, 125(2), 114–126. https://doi.org/10.1111/j.1600-0447.2011.01786.x
3. Albajara Sáenz, A., Villemonteix, T., & Massat, I. (2019). Structural and functional neuroimaging in attention-deficit/hyperactivity disorder. Developmental Medicine & Child Neurology, 61(4), 399–405. https://doi.org/10.1111/dmcn.14050
4. Saad, J. F., Griffiths, K. R., & Korgaonkar, M. S. (2020). A systematic review of imaging studies in the combined and inattentive subtypes of attention deficit hyperactivity disorder. Frontiers in Integrative Neuroscience, 14, 31. https://doi.org/10.3389/fnint.2020.00031
5. Shook, D., Brady, C., Lee, P. S., Kenealy, L., Murphy, E. R., Gaillard, W. D., VanMeter, J. W., Cook Jr, E. H., & Vaidya, C. J. (2011). Effect of dopamine transporter genotype on caudate volume in childhood ADHD and controls. American Journal of Medical Genetics Part B: Neuropsychiatric Genetics, 156B(1), 28–35. https://doi.org/10.1002/ajmg.b.31132
6. Pineda, D. A., Restrepo, M. A., Sarmiento, R. J., Gutierrez, J. E., Vargas, S. A., Quiroz, Y. T., & Hynd, G. W. (2002). Statistical analyses of structural magnetic resonance imaging of the head of the caudate nucleus in Colombian children with attention-deficit hyperactivity disorder. Journal of Child Neurology, 17(2), 97–105. https://doi.org/10.1177/088307380201700202
7. Milham, M. P., Fair, D., & Nigg, J. T. (2012). The ADHD-200 Consortium: A model to advance the translational potential of neuroimaging in attention deficit hyperactivity disorder. Frontiers in Systems Neuroscience. https://www.ncbi.nlm.nih.gov/pmc/articles/PMC3433679/
8. Brown, M. R. G., Sidhu, G. S., Greiner, R., Asgarian, N., Bastani, M., Silverstone, P. H., Greenshaw, A. J., & Dursun, S. M. (2012). ADHD-200 Global Competition: diagnosing ADHD using personal characteristic data can outperform resting state fMRI measurements. Frontiers in Systems Neuroscience, 6, 69. https://doi.org/10.3389/fnsys.2012.00069
9. Peng, X., Lin, P., Zhang, T., & Wang, J. (2013). Extreme learning machine-based classification of ADHD using brain structural MRI data. PLoS ONE, 8(11), e79476. https://doi.org/10.1371/journal.pone.0079476
10. Zhang-James, Y., Razavi, A. S., Hoogman, M., Franke, B., & Faraone, S. V. (2023). Machine learning and MRI-based diagnostic models for ADHD: Are we there yet? Journal of Attention Disorders, 27(4), 335–353. https://doi.org/10.1177/10870547221146256
11. Thomson, P., Loosley, V., Friedel, E., et al. (2024). *Changes in MRI head motion across development: Typical development and ADHD. Brain Imaging and Behavior, 18*, 1144-1152. https://doi.org/10.1007/s11682-024-00910-w
12. Ahmed, M. A., Moftah, H. M., & Mahmoud, H. A. (2025). *Deep learning for interpretable ADHD diagnosis from fMRI: ConvLSTM with enhanced augmentation, Grad-CAM explainability, and external validation. International Journal of Computational and Experimental Science and Engineering, 11*(3). https://doi.org/10.22399/ijcesen.3864
13. Dai, Y.-W., & Hsu, C.-F. (2025). *Machine learning for ADHD diagnosis: Feature selection from parent reports, self-reports and neuropsychological measures. Children, 12(*11), 1448. https://doi.org/10.3390/children12111448
14. Lohani, D. C., Chawla, V., & Rana, B. (2025). A systematic literature review of machine learning techniques for the detection of attention-deficit/hyperactivity disorder using MRI and/or EEG data. Neuroscience, 570, 110–131. https://doi.org/10.1016/j.neuroscience.2025.02.019
15. Pecci-Terroba, C., et al. (2025). *Subgrouping autism and ADHD based on structural MRI population modelling centiles. Molecular Autism, 16,* 33. https://doi.org/10.1186/s13229-025-00667-z